Fracture morphology pattern transition dominated by the crack tip curvature radius in brittle metallic glasses

M. Gao, D.W. Ding, D.Q. Zhao, H.Y. Bai, W.H. Wang *

Institute of Physics, Chinese Academy of Sciences, Beijing 100190, China

A R T I C L E   I N F O

A B S T R A C T

The dynamic evolutions of different fracture morphologies in the fracture surface of brittle Mg-based metallic glasses (MGs) were systematically and quantitatively studied by SEM and AFM. It shows that the evolution of the fracture morphology pattern is dominated by an effective dynamic parameter of critical crack tip curvature radius. Based on crack tip plastic zone and shear transformation zone (STZ) theories, a theoretical model for the evolution of the crack tip curvature radius by considering the activation of STZs during fracture was proposed. The model can simulate the crack propagation process, and predict the critical crack tip curvature radius and the fracture pattern transition between the dimples and the periodic corrugations solely occurring in brittle MGs. These results have implications for understanding the microscopic fracture mechanism and the structural origin of fracture in MGs.

© 2014 Elsevier B.V. All rights reserved.

1. Introduction

Spatiotemporal patterns in nature, such as sweeping loops of meandering rivers, crescent and star-shaped patterns of sand dunes, and convective patterns of normal fluids, offer a direct clue to understand the dynamic behaviors of non-equilibrium systems [1–3]. The catastrophic brittle fracture of glasses, as a typical non-equilibrium process, is one of the most poorly understood fundamental phenomena in condensed matter physics [4,5]. The disordered structure makes glasses exhibit much different and unique dynamic fracture patterns compared with those of crystalline materials [6,7]. Particularly, for metallic glasses (MGs) combining the glassy structure and nature, and metallic bonds, various and plentiful dynamic fracture patterns like dimple structures [8], periodic corrugations [9], and river patterns [8] appear selectively in different regions of their fracture surface. The formation and evolution of these fracture patterns in fracture surface is a favorable fingerprint to discover the unknown crack propagation process and fracture mechanism in glasses. In addition, the micro-scale and nano-scale fracture structure such as striped structure might have potential applications in the nano-scale grating and templates. However, the key factor controlling the formation and evolution of these structures is still unclear.

The appearance of typical fracture morphology of dimple structures suggests that the microscopic plastic deformation at crack tip dominates the cracking process and the fracture pattern formation in brittle MGs. However, there is no complete theoretical scheme to understand the plastic deformation at crack tip, and the reasons for the MGs with diverse fracture toughness and completely different fracture morphology are still unknown. The plastic deformation of MGs is widely described by the cooperative shearing of atomic clusters termed shear transformation zones (STZs) [10], and the operation and proliferation of the flow units of STZs further induce the drop in viscosity and the formation of liquid-like zone at crack tip during fracture [11]. The STZ model proposed by Argon [10] and further developed by Langer et al. [12–14] is a systematic formulation of non-equilibrium thermodynamics and captures many plastic deformation behaviors in glassy materials. Recently, Bouchbinder et al. applied the STZ theory to explain the tip blunting and velocity selection in dynamic fracture [15]. Rycroft et al. used a simple version of STZ model to calculate the fracture toughness and understand the annealing-induced embrittlement of MGs [16]. The universal fractal nature of the dimple structures in fracture surface of various MGs can be illustrated properly by the athermal STZ theory [17]. These results indicate that the STZ may be considered as the microscopic deformation unit of fracture process, and the STZ theory may be used as a theoretical frame to understand the fracture pattern formation and transition in MGs [18,19].

The microscopic formation mechanism of the diverse fracture morphology in MGs remains unclear. Especially, the effective parameter which can be used to characterize the dynamic crack propagation is lacking. Previous researches on the fracture morphology evolution of MGs mainly focused on the average space or depth of typical patterns, and these parameters hardly revealed the dynamic information of the crack propagation [20–22]. Recent

researches [23,24] show that the crack tip curvature radius and the crack propagation velocity are relevant dynamical variables during dynamic fracture, which could dominate the crack propagation and control the fracture pattern transition in MGs, while their relationship has been less studied experimentally and theoretically.

In this paper, the brittle $Mg_{65}Cu_{25}Gd_{10}$ MG (toughness $K_C=$ 2 MPa m$^{1/2}$) was selected as a model system since various fracture patterns appear in its fracture surface. The fractographic evolution and the corresponding crack tip curvature radius evolution during crack propagation are investigated by a new parameter of crack tip curvature radius. We find that there exists a critical crack tip curvature radius controlling the pattern transition from the dimple structures to the periodical corrugations. A theoretical scenario based on the truncated version of the STZ theory is proposed to understand the dynamical evolution of crack tip curvature radius and the mechanism of fracture pattern transition in brittle MGs. These results might provide useful insight into the fracture mechanism of MGs and could be generally applicable to other glassy materials.

2. Experimental

The brittle $Mg_{65}Cu_{25}Y_{10}$ metallic glass ingots were prepared by induction melting a mixture of pure metal elements, followed by sucking cast into a Cu mold under argon gas atmosphere to get the plate-like specimens $5 \times 3 \times 60$ mm^3 in geometric size. The amorphous structures of the samples were identified by a Rigaku X-ray diffractometer (XRD) with Cu K_α radiation and differential scanning calorimetry. The three-point bending tests were carried out in an Instron 3384 machine (Norwood, MA) with a crosshead moving speed of 0.1 mm min^{-1} at room temperature. The bending test was repeated three times to confirm the experiment results. Specimens for pre-notched three-point bending tests had a geometric size $3 \times 2 \times 15$ mm^3. A diamond saw was used to introduce a seed notch (250 μm in width and 500 μm in depth) in the center of the plates. The newly created fracture surfaces were observed by a Philips XL30 scanning electron microscopy (SEM) instrument with the high resolution of 1.5 nm and a Oxford Instruments MFP-3D Stand Alone atomic force microscope (MFP-3D-SA AFM).

3. Results and discussion

3.1. SEM observation of fracture morphology in fracture surface

Fig. 1(a) shows the typical mirror-like fracture surface profile of the Mg-based MG. The fracture surface clearly displays the distinct river-like, mist, mirror zones along the crack propagation direction similar to previous reports [9,11,20]. The fractographic evolution sequence is the dimples in river-like zone b [Fig. 1(b)], the dimple and periodical corrugation mixed structures in mist zone c [Fig. 1(c)], and
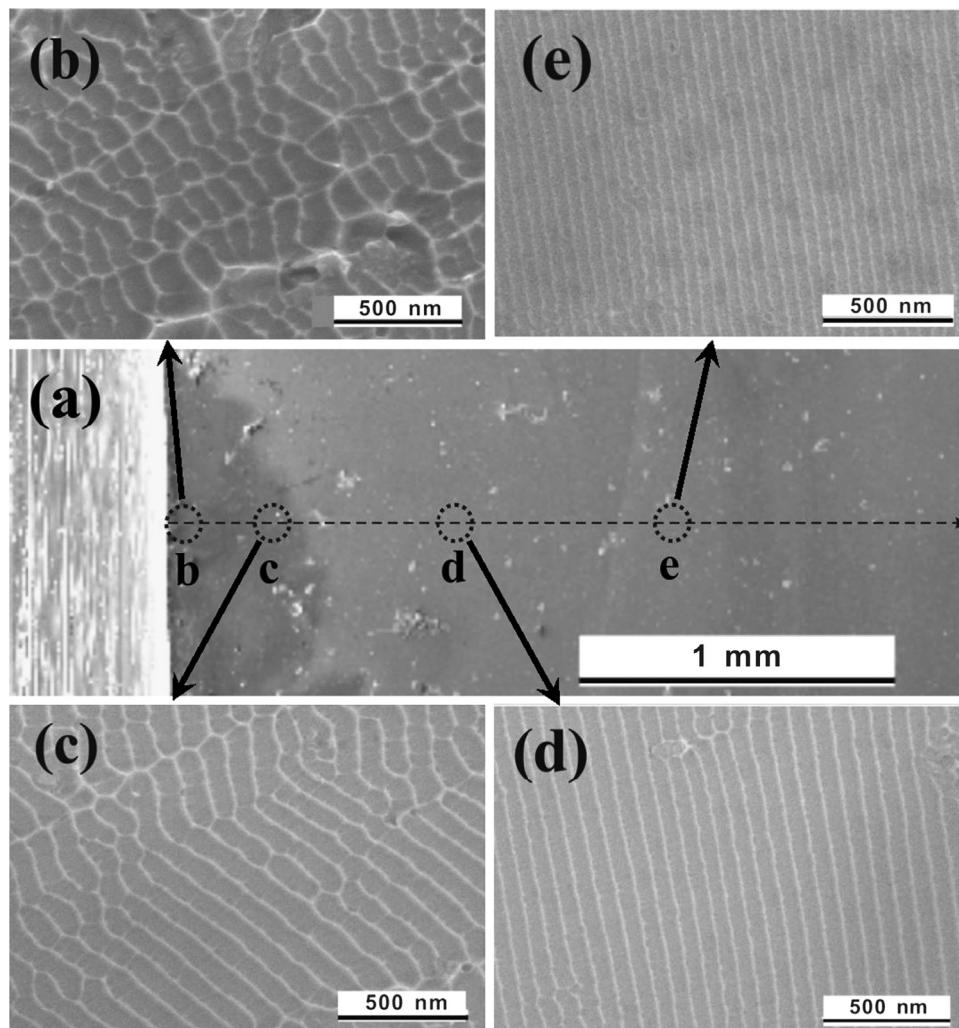
Fig. 1. (a) Overview of the fracture surface of $Mg_{65}Cu_{25}Y_{10}$ under three-point bending fracture (the dashed arrow indicates the crack propagation direction). (b)–(e) Detail morphology of zone b, zone c, zone d, zone e in (a), correspondingly.

periodical corrugations in mirror zones d and e [Fig. 1(d) and (e)]. It has been demonstrated that the main fracture surface features remain unchanged except the relative space ranges of different fracture pattern zones that change upon the fracture strain rate [8,9]. The SEM images in Fig. 1 show that the typical size of each fracture pattern shows no large variation. Obviously, the different fracture morphology zones correspond to the different pattern formation stages in dynamical fracture of the brittle MGs.

3.2. AFM characterization of various fracture patterns in fracture surface

The AFM was applied to quantitatively characterize the fracture morphology evolution with the crack propagation distance L from the notch. Fig. 2 shows the evolution of the average spacing d and the depth h of the various fracture patterns, and the data of each fracture pattern are also listed in Table 1. Obviously, the d decreases continuously from the river-like zone to the mirror zone and the depth h remains unchanged at $L \approx 1000\ \mu m$, which is consistent with previous studies [20,22]. However, when $L \approx 2000\ \mu m$ as indicated in Fig. 2, the pattern transition from the dimple to the periodic corrugation appears, indicating that the parameters d and h can hardly reveal the fracture pattern transition mechanism in brittle MGs. Next, we attempt to introduce a new dynamical variable of crack tip curvature radius R_C to effectively evaluate the crack propagation process as the following.

Owing to the large deviation in determining the crack tip curvature radius R_C experimentally, another experimentally obtained dynamic parameter κ having a positive correlation with R_C is proposed as below. Based on the crack tip plastic zone model and
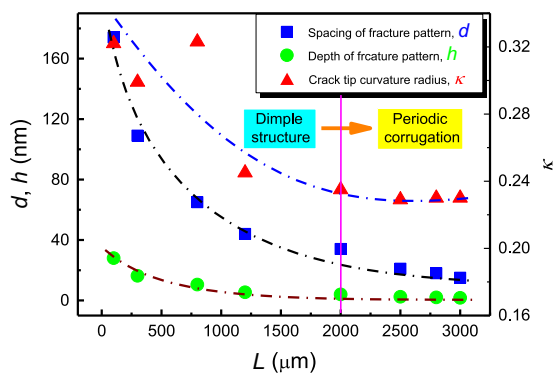
Fig. 2. Average spacing d, depth h and dynamic parameter κ of different fracture patterns as functions of crack propagation distance L are displayed by the black, wine and blue dash–dot lines, respectively. The pink vertical line indicates the location of fracture morphology transition from the dimple structures to the periodic corrugations. (For interpretation of the references to color in this figure legend, the reader is referred to the web version of this article.)

Table 1
The data of different fracture patterns in fracture surface measured by AFM. L is the crack propagation distance from the notch edge site to the measurement site; d and h are the average size and the depth of fracture patterns, respectively; κ is the ratio value between $d/2$ and h, which is equivalent to crack tip curvature radius.

L (μm)	d (nm)	h (nm)	κ	Fracture patterns
~100	174	28	0.322	Dimple structure
~300	109	16.3	0.299	Dimple structure
~800	65	10.5	0.323	Mixture structure
~1200	44	5.4	0.245	Mixture structure
~2000	34	4	0.235	Mixture structure
~2500	21	2.4	0.229	Periodic corrugation
~2800	18	2	0.23	Periodic corrugation
~3000	15	1.7	0.23	Periodic corrugation

previous experimental results [11,25], the up–down corresponding fracture surfaces of MGs show the peak-to-peak matching style, which indicates that a sequence of fracture morphologies starts from the cavitations by the progressive local separation in the plastic zone as shown in Fig. 3(a). Bouchaud et al. [26] also got the similar experimental results by using the Frasta method to reconstruct the cavity formation during the fracture process. Compared to the irregular fracture morphologies in ductile MGs [21,26], the cavitations leading to the formation of fracture patterns of brittle MGs are regular and quasi-periodic as shown in Fig. 1 and based on the previous research [22]. Therefore, these cavitations can be well described by a regular geometric model: that is the ellipse configuration. Considering the actual value of the spacing and depth of the fracture patterns listed in Table 1, we could reasonably consider the cavitations leading to the formation of dimple structures and periodic corrugations as a series of elliptic holes in the left part in Fig. 3(a). And the half values of spacing $d/2$ and depth h are considered as the major radius and minor radius of the elliptic hole respectively as shown in Fig. 3(b). Due to the small value of the ratio between d and h, the ratio between the major radius and minor radius, $\kappa = h/(d/2) = \tan\varphi$, should be approximately proportional to φ, that is, $\kappa = \tan\varphi \propto \varphi$. During the crack propagation process, the crack tip curvature radius R_C varies dynamically and the parameter φ displays the same trend with R_C concomitantly considering the geometric character of the elliptical hole. Thus, the variable κ exhibits the same tendency with R_C during the whole dynamic fracture process, and then can be used to characterize the evolution of fracture patterns and plays the same role with R_C. It is noted that this approximation may be convenient and effective in experimental date processing, and the approximation might be applied to study other fracture problems, such as the structural origin of nanoscale cavitations during the deformation of MGs [27].

Fig. 2 also shows the evolution of the dynamic variable κ along the crack propagation direction. One can see clearly that κ exhibits a large decrease when the pattern changes from the dimple structures to the periodic corrugations and then keeps a stable value. This reveals that there is a critical value of κ controlling the fracture pattern evolution, which indicates physically that there is a critical R_C separating the dimple pattern from the periodic stripe pattern. And the different R_C regimes described above might correspond to the common mirror–mist–hackle transition, a fractographic characterization which corresponds to the progressive increase in surface roughness with the crack speed [8,9,11]. These results are also consistent with the appearance of the critical crack propagation velocity and the drop in the stress intensity factor during the transition between the dimple structures and the periodic corrugations [22,25,28]. The existence of the critical crack tip curvature radius R_C may be used to tune the appearance of different fracture patterns in fracture surface of MGs. To further understand the fracture pattern transition mechanism and the appearance of the critical R_C, we propose a theoretical model of the fracture process in brittle MGs based on the STZ theory.

3.3. The model of the dynamic fracture in brittle MGs based on STZ theory

Theoretically solving the dynamic crack propagation problem is in general extremely difficult due to the coupling between various parameters across different scales in fracture including the typical size of the crack tip plastic zone and the scale of STZs, which are two main factors governing the dynamic fracture of MGs [8,11,22,29]. A promising theoretical scheme of the dynamics fracture in amorphous materials was proposed recently by Larger [30,31]. By considering the crack tip curvature radius R_C and the crack propagation speed v_{tip} as the relevant dynamical variables and considering the crack advance as a process governed solely by
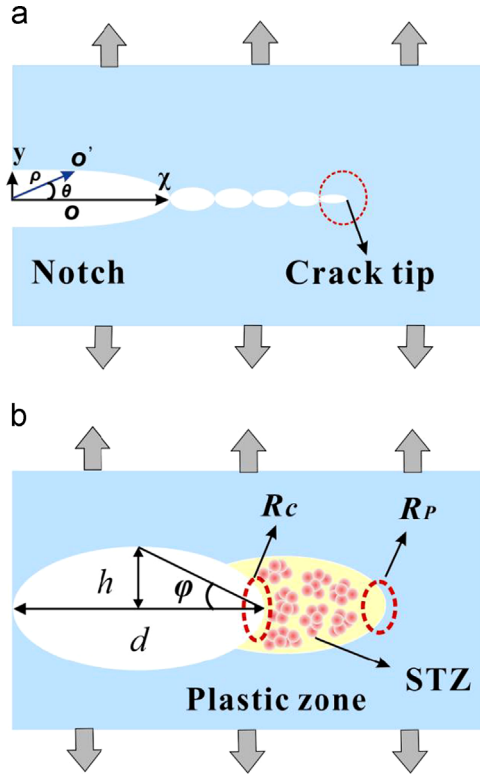
Fig. 3. (a) Sketch of the formation mechanism of fracture patterns of brittle MGs. The string of ellipses starting from the notch represent the holes generated during the crack propagation, leading to the formation of different fracture patterns. In the notch, the Cartesian coordinates (x, y) and the elliptical coordinates (ρ, θ) are both shown. (b) Microscopic physical model of crack tip [region circled by the red dashed circle in (a)]. R_C is the crack tip curvature radius. R_P is the curvature radius of the plastic zone at crack tip. φ is the angle in the elliptic hole model having a positive correlation with the crack tip curvature radius. The fracture groove points are inward in the illustration. (For interpretation of the references to color in this figure legend, the reader is referred to the web version of this article.)

plastic deformation at crack tip, the tip-stress puzzle between the conventional theories of plasticity and the descriptions of brittle fracture could be understood. Here, we propose a model for the crack tip curvature evolution during fracture of brittle MGs based on the STZ theory of brittle fracture [30–32] to grasp the microscopic fracture mechanism and the formation mechanism of fracture surface morphologies.

3.3.1. Microscopic physical picture of the crack tip evolution during fracture in brittle MGs

Compared with the tough MGs which exhibit a much larger scale of local plasticity and significant crack bifurcation and micro-branching [28], brittle MGs such as Mg-, Dy- and Fe-based MGs approaching the ideal brittleness of silicate glasses display the nano-scale crack-tip plasticity and no obvious micro-branching instability [8], which leads to the formation of regular fracture patterns and the stable crack propagation in every pattern formation stage. This indicates that there exists a weak stress-dependent factor influence in plastic zone of crack tip during fracture in brittle MGs. Therefore, the basic approximation of brittle fracture in amorphous materials based on the STZ theory in Ref. [32], where a strongly stress-dependent rate factor governing memory effects of plastic deformation could be omitted in brittle fracture, is very suitable for the fracture process in brittle MGs. According to the approximation, the dynamic variables R_C and v_{tip} could be regarded to be completely determined by the crack tip plastic zone [11], and thus be governed solely by the plastic deformation at

crack tip, which greatly reduces the factors influencing the fracture process and crack propagation in our model.

In our previous work [17], a microscopic picture for the formation of the plastic zone at crack tip considering the creation and annihilation of STZs is proposed to explain the fractal nature of the dimples structures of different MGs with different fracture toughness. Here, a physical model of the dynamic evolution of the crack tip in brittle MGs is proposed based on the above picture: firstly, some initial STZs are activated with the effect of the shear stress s in the neighborhood zone of crack tip during fracture. The operation of these STZs creates a localized softening of the surrounding material and triggers the autocatalytic formation of more STZs at the crack tip. The organization of STZs coalesces together into a softening zone – the plastic zone – during fracture. During the dynamic fracture, STZs in plastic zone at crack tip create and annihilate continuously, which induces the dynamic evolution of the stress s and the rate-of-deformation $\dot{s}^{pl}$ in plastic zone at crack tip. And the dynamic evolution of the plastic zone at crack tip shows the dynamic evolution of R_C and v_{tip}, which directly leads to the fracture patterns formation and transition during fracture. Thus, it is the activation (creation and annihilation) of STZs in MGs that controls completely the crack propagation of MGs and the fracture pattern transition during fracture as exhibited in Fig. 3(b). The R_C is the crack tip curvature radius, and the R_P stands for the curvature radius of the plastic zone at crack tip as indicated in Fig. 3(b). During fracture, the R_C and R_P evolve separately and the actual fracture process is a discontinuous and step-by-step process [22]. However, considering the effect of the crack tip configuration on the following plastic zone formation [23], we could approximately regard the spatial evolution of R_C during fracture as a continuous change process. That is, the $R_P(t)$ of the plastic zone at time t could be considered as the crack tip curvature radius $R_C(t+\Delta t)$ in following time $(t+\Delta t)$ during fracture. Δt is the time interval that the crack tip propagates from the location of $L(t)$ to the location $L(t+\Delta t)$. The time interval Δt should be short enough to consider the crack tip evolution process as a continuous process compared to the experimental observation time $\Delta t'$. To make this model more suitable for the dynamic fracture of brittle MGs, the crack tip profile is approximately regarded as a highly elongated elliptical hole rather than a circular hole in conventional fracture problems, and the crack tip remains elliptical during fracture. Considering that the above experimental dynamic variable κ is small during the whole crack propagation, the elliptical approximation is physically reasonable. Based on the above model of the plastic zone at crack tip and the quasi-static three-point bending experimental conditions, the truncated STZ theory omitting strongly stress-dependent rate factor [32] can be applied reasonably to analyze the dynamical crack tip evolution of brittle MGs.

3.3.2. Theoretical brittle fracture model based on the STZ theory

Based on the STZ theory [31], the dynamic evolution of the stress and the rate-of-deformation during fracture are in the two coupled main equations:

$$\dot{\varepsilon}^{pl} \approx \frac{1}{\tau}(\lambda s - \Delta) \tag{1}$$

$$\dot{\Delta} \approx \dot{\varepsilon}^{pl} - \left(\frac{\dot{\varepsilon}^{pl}s}{\lambda s_y^2}\right)\Delta. \tag{2}$$

Here, $\dot{\varepsilon}^{pl}$ is the plastic strain rate, s the deviatoric stress, s_y is the yield stress, Δ is a tensor describing the anisotropy in the STZ's orientations, λ is a parameter of dimension inverse stress that measures the plastic strain rate sensitivity to stress, and τ is a typical time scale for atomic rearrangement.

To calculate conveniently the variables of the elliptical crack tip configuration during fracture, the Cartesian coordinates (x, y) are transformed into the elliptical coordinates (ρ, θ) by $x = W(\rho + m/\rho)\cos\theta$ and $y = W(\rho - m/\rho)\sin\theta$ as shown in the left part in Fig. 3(a), where m and W are variables describing the elliptical hole profile. The semimajor and semiminor axe lengths of the ellipse hole are $W(1 + m)$ and $W(1 - m)$ respectively and $1 > m > 0$. The stress tensor σ and the rate of plastic strain tensor D in the neighborhood of the elliptical hole can be got based on Ref. [33] and have been calculated in Ref. [32]. The stresses σ in the neighborhood of the elliptical hole are

$$\sigma_{\rho\rho} + \sigma_{\theta\theta} = \sigma_\infty \text{Re}\left[1 + \frac{2(1+m)e^{-2i\theta}}{\rho^2 - me^{-2i\theta}}\right] \tag{3}$$

$$
\begin{aligned}
S(\rho, \theta) &= \sigma_{\theta\theta} - \sigma_{\rho\rho} + 2i\sigma_{\rho\theta} \\
&= \frac{\sigma_\infty \rho^2 e^{2i\theta}}{\rho^2 - me^{2i\theta}}\left[1 - \frac{e^{-2i\theta}}{m\rho^2} + \frac{(1+m)e^{-2i\theta}}{(\rho^2 - me^{-2i\theta})^2}M(\rho, \theta)\right]
\end{aligned} \tag{4}
$$

where $M(\rho, \theta) = (\rho^2/m)(1 - 2me^{-2i\theta} + m^2) + e^{-2i\theta}(1 - 2me^{2i\theta} + m^2)$, and the deviator stress

$$s_{\theta\theta} = -s_{\rho\rho} = \frac{1}{2}\text{Re}S(\rho, \theta), s_{\rho\theta} = \frac{1}{2}\text{Im}S(\rho, \theta). \tag{5}$$

And the rate-of-deformation tensors D are [32]

$$D_{\rho\rho} = \frac{1}{WN}\left(\frac{\partial v_\rho}{\partial \rho} + \frac{v_\theta}{\rho}\frac{1}{N}\frac{\partial N}{\partial \theta}\right) \tag{6}$$

$$D_{\theta\theta} = \frac{1}{WN\rho}\left(\frac{\partial v_\theta}{\partial \theta} + \frac{v_\rho}{\rho}\frac{1}{N}\frac{\partial}{\partial \rho}(\rho N)\right) \tag{7}$$

$$D_{\rho\theta} = \frac{1}{2WN}\left(\frac{1}{\rho}\frac{\partial v_\rho}{\partial \theta} + \frac{\partial v_\theta}{\partial \rho} - \frac{v_\theta}{\rho} - \frac{v_\rho}{N}\frac{\partial N}{\partial \theta} - \frac{v_\theta}{N}\frac{\partial N}{\partial \rho}\right) \tag{8}$$

where $N^2(\rho, \theta) = 1 + (m^2/\rho^4) - 2(m/\rho^2)\cos 2\theta$, v_ρ and v_θ are the radial and angular velocities in the elliptical hole respectively. Eqs. (3)–(8) are the basic functions controlling the stresses and the rate-of-deformation tensors in the neighbor of holes at crack tip and these equations are universal during brittle fracture in amorphous materials [32,33].

In order to determine the motion of the elliptical crack tip, the normal velocity on the surface at crack tip ($\rho = 1$, $\theta = 0$), $v_n(\theta)$ needs to be computed, that is, the crack propagation velocity v_{tip}, and the rate of change of the curvature of the crack tip surface $\dot{K}$. The two dynamic parameters can be calculated from Eqs. (1) to (8) based on the approximation that the normal velocity at crack tip $v_n(\theta)$ is $(\lambda/\tau)K^{-1}(\theta)[s_{\theta\theta}(1, \theta) - s_y]$ for $s_{\theta\theta} > s_y$ and zero for otherwise, which means that the angular velocity v_θ vanishes and the plastic flow is purely radial. During fracture of brittle MGs, the fracture surfaces are almost flat and mirror-like, and the crack tip propagates along the main fracture plane surface, which means that the radial velocity dominates the crack propagation during fracture. Thus, based on the above analysis of the fracture process in brittle MGs, this approximation seems to be well satisfied in our model. The crack propagation velocity v_{tip}, and the rate of change of the curvature of the crack tip surface $\dot{K}$ are (the detailed calculations can be seen in Ref. [32])

$$v_{tip} = v_{\rho=1}(\theta = 0) \cong \frac{\lambda}{\tau}\left(\sigma_\infty\sqrt{\frac{2W}{K_{tip}}} - \frac{s_y}{K_{tip}} - c\gamma\right) \tag{9}$$

$$\dot{K}_{tip} \cong \frac{2\lambda}{\tau}(-\sigma_\infty\sqrt{2W}K_{tip}^{3/2} + 2s_yK_{tip} - d\gamma K_{tip}^2), \tag{10}$$

where W is one-quarter of the major length of the ellipse hole (in fracture surface of MGs, $4W$ is the typical size of the dimple structure considering the highly elongated elliptical hole model and the above transformation relation between the elliptical

coordinates and the Cartesian coordinates); σ_∞ is the applied stress at infinity; γ the surface tension; c and d are the numerical coefficients. From Eq. (10), considering the relationship between K_{tip} and R_{tip}, $K_{tip} = 1/R_{tip}$, we can get the expression of the evolution process of the crack tip curvature radius R_{tip}:

$$\dot{R}_{tip} = -\frac{4\lambda}{\tau}s_yR_{tip} + \frac{2\lambda}{\tau}\sigma_\infty\sqrt{2W}R_{tip}^{1/2} + 2d\gamma\frac{\lambda}{\tau}. \tag{11}$$

Eqs. (9) and (11) can completely describe the evolution process of the crack propagation velocity and the crack tip curvature radius, and meanwhile control the patterns transition among different fracture morphologies.

3.3.3. Critical crack tip curvature radius calculations based on the model of the dynamic fracture in brittle MGs

By analyzing Eqs. (9) and (11), one can find there exists a steady crack tip curvature radius R_{tip}^* and a crack velocity v_{tip}^* [32] during the dynamic fracture. By setting the right part of Eq. (11) zero and we can get the steady value of R_{tip}:

$$R_{tip}^* = \frac{1}{2Wk^{*2}}\frac{\gamma^2}{\sigma_\infty^2} \tag{12}$$

$$v_{tip}^* = \frac{\lambda\gamma}{\tau}\left(\frac{1}{k^*} - c - \frac{1}{2gk^{*2}}\right) \tag{13}$$

where $k^* = (1/2d)(\sqrt{1 + (4d/g)} - 1)$, $g = (W\sigma_\infty^2/\gamma s_y)$. This result is consistent with the experimental result that there exists the steady crack propagation velocity in fracture of brittle MGs. From Eq. (12), we can get

$$
\begin{aligned}
R_{tip}^* &= \frac{1}{2W\left[(1/2d)(\sqrt{1 + (4d/g)} - 1)\right]^2}\frac{\gamma^2}{\sigma_\infty^2} \\
&= \frac{2d^2}{W\sigma_\infty^2}\frac{\gamma^2}{(\sqrt{1 + (4d/g)} - 1)^2}
\end{aligned} \tag{14}
$$

By introducing the expression of g, we can transform Eq. (14) into

$$
\begin{aligned}
R_{tip}^* &= 2d^2\frac{\gamma}{s_y}\frac{\gamma s_y}{W\sigma_\infty^2}\frac{1}{(\sqrt{1 + (4d/g)} - 1)^2} \\
&= \frac{\gamma}{s_y}\frac{2d^2}{g}\frac{1}{(\sqrt{1 + (4d/g)} - 1)^2}
\end{aligned} \tag{15}
$$

Taking the values of the relevant parameters into Eq. (15), we obtain the values of g which are listed in Table 2. From the values of g in Table 2, we can calculate the average value of g for various brittle MGs: $g_{average} \approx 62$, with a standard error value of about 1.84. As shown in the inset in Fig. 4, the value of g can be considered as a constant for different brittle MGs. It should be noted that the value of g for $Zr_{57}Nb_5Cu_{15.4}Ni_{12.6}Al_{10}$ (typical tough MG) is about 6.5×10^3, and is far from the average value of g of brittle MGs, which indicates that our fracture model may not be applicable for tough MGs. Based on the above analysis, Eq. (15) can be changed into

$$R_{tip}^* = \frac{\gamma}{s_y}A_0 \tag{16}$$

where $A_0 = (2d^2/g)(1/(\sqrt{1 + (4d/g)} - 1)^2)$, a constant for various brittle MGs. Thus, Eq. (16) can be written into

$$R_{tip}^* \propto \frac{\gamma}{s_y}. \tag{17}$$

This result is consistent with the experimental result of $R_{tip}^* \approx 1024(\gamma/G)$ [22] considering the relationship $s_y \approx \varepsilon_C G$ (G is the shear

Table 2

Critical crack tip curvature radius from calculations R_{tip}^* and experiments R_{exp}^* [22], activation energy of STZs $E_{STZ} \sim 0.39 G V_m$ calculated based on cooperative shear model [18,34] in MGs with different fracture toughness K_{IC}. Values of parameter g in Eq. (13) can be calculated by $g = (W \sigma_y^2 / \gamma \varepsilon_y G)$. Data of K_{IC}, G, and V_m are from Ref. [35].

Metallic glasses	K_{IC} (MPa m$^{1/2}$)	G (GPa)	V_m (cm^3/mol)	E_{STZ} (kJ/mol)	g	R_{exp}^* (nm)	R_{tip}^* (nm)	Brittle or tough
Dy$_{40}$Y$_{16}$Al$_{24}$Co$_{20}$	1.26	4.4	13.54	128.8	62.4	42	51	Brittle
Mg$_{65}$Cu$_{25}$Tb$_{10}$	~2	9.6	11.96	91.4	60.4	41.5	42.4	Brittle
Mg$_{65}$Cu$_{25}$Gd$_{10}$	~2	9.3	12.50	94.1	59.3	34	39	Brittle
Fe$_{65.5}$Cr$_4$Mo$_4$Ca$_4$P$_{12}$C$_5$B$_{5.5}$	~2	8.5	6.71	153.1	63.4	26	28.7	Brittle
Fe$_{73.5}$Cu$_1$Nb$_3$Si$_{13.5}$B$_9$	2.7	8	6.86	181.9	62	30	28.2	Brittle
La$_{55}$Al$_{25}$Ni$_5$Cu$_{10}$Co$_5$	5	5.6	16.15	92.9	58.8	60	73	Brittle
Zr$_{57}$Nb$_5$Cu$_{15.4}$Ni$_{12.6}$Al$_{10}$	27	2	11.44	142.8	6.5×10^3	46.5	5.6×10^3	Tough
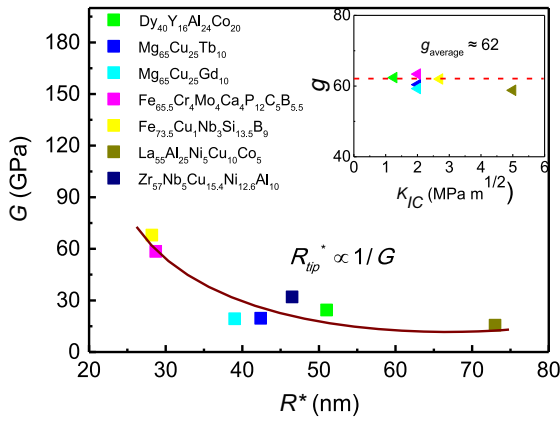
Fig. 4. The relationships of critical crack tip curvature radius R_{tip}^* and shear modulus G. The wine curve stands for the fitting curve of $R_{tip}^* \propto 1/G$. The inset shows the values of the intermediate parameter g in Eq. (13) of brittle MGs with different fracture toughness. The red dashed line represents the average value of g of six brittle MGs (the value of g of tough Zr$_{57}$Nb$_5$Cu$_{15.4}$Ni$_{12.6}$Al$_{10}$ MG is not included in this plot), about 62. (For interpretation of the references to color in this figure legend, the reader is referred to the web version of this article.)

Fig. 5. Critical crack tip curvature radius from calculations R_{tip}^* and experiments R_{exp}^* of seven MGs. The red dashed line represents the boundary between the brittle and tough MGs. (For interpretation of the references to color in this figure legend, the reader is referred to the web version of this article.)

modulus; ε_C is a constant as following) indicating that our dynamic fracture model is justifiable. The relationship $R_{tip}^* \propto (\gamma/G)$ can be easily understood in MGs since the fracture process involves breaking of liquid-like meniscus at crack tip and then the factor γ plays a critical role. The plastic deformation at crack tip causes the formation of the plastic zone and then dominates the dynamic evolution of fracture morphology, where the factor G reflects the effect of plastic deformation during fracture. Thus, this relationship actually reflects the competition relationship between the two processes – the meniscus instability (Ref. [11]) and the plastic deformation at crack tip-deciding the crack tip evolution. These analyses are approximately consistent with our dynamic fracture model for brittle MGs in experiments.

To conveniently estimate the value of R_{tip}^*, we let $s_y \approx \varepsilon_C G$, where G is the shear modulus and ε_C is the universal elastic strain limit (~0.0267 in Ref. [34]) for all MGs, and this relationship has been confirmed by the previous theoretical and experimental research [34,35]. For MGs, the typical values of γ for various brittle MGs are in the order of 0.7–1 N/m [22] and then γ could approximately be considered as a constant. Therefore, the values of R_{tip}^* are roughly proportional to $1/G$, as shown in Fig. 4:

$$R_{tip}^* \propto \frac{1}{G}. \tag{18}$$

The simple relationship indicates that one could obtain the various fracture patterns by tuning simply the shear modulus of MGs. We note that in elastic model [34,35], the activation energy of STZs is mainly determined by G. The obtained relationship of

Eq. (18) further confirms the close relationship between the STZ and plastic zone at the tip of crack in brittle MGs.

For Mg$_{65}$Cu$_{25}$Gd$_{10}$ MG, $\sigma_\infty = \sigma_y = 660$ MPa, $s_y \approx \varepsilon_C G = 0.52$ GPa, $\gamma = 0.7$ N/m, $c = 0.5$ and $d = 1$. Considering the highly elongated elliptical hole of crack tip plastic zone, the major length of the ellipse hole $4W$ is the typical size of the dimple of 200 nm for the MGs [8]. The experimental critical crack propagation velocity of the MGs v_C is about 0.3–0.6$v_R \approx 1247$ m/s [21,36], where v_R is the Rayleigh wave speed ($v_R \approx 0.9225 v_S$, v_S the shear wave velocity). The numerical coefficients c and d are 0.5 and 1, respectively. Taking the values of these variables into Eq. (13), we get $\lambda/\tau \approx 60$. Thus, the value of R_{tip}^* estimated from Eq. (12) is ~39 nm, which fits very well with the experimental result of 34 nm. The R_{tip}^* of other brittle MGs are also estimated and listed in Table 2. Fig. 5 shows a comparison between the estimated R_{tip}^* and the experimental R_{exp}^* for various brittle MGs. Apparently, the R_{tip}^* from our model fits well with the experimental results for brittle MGs. We note that our model based on the STZ coalescence and cavitation in plastic zone is invalid for tough MGs. For tough Zr-based MG, the large deviation appears between the theoretical and experimental results as shown in Fig. 5. Considering the above omission of strongly stress-dependent rate factor governing memory effects of plastic deformation and the microscale local plastic zone of tough MGs, the deviation is reasonable since the strongly stress-dependent rate factor plays a more critical role in fracture of tough MGs, leading to a significant crack bifurcation and branching.

3.3.4. Crack tip sharpening and blunting phenomena

We further study the qualitative evolution of the R_{tip} with different initial crack tip curvature radii R_{tip}^0 during the whole dynamic fracture. Considering the succinctness of the equation, let

$A = (2\lambda/\tau)2s_y$, $B = (2\lambda/\tau)\sigma_\infty\sqrt{2W}$, $C = d\gamma(2\lambda/\tau)$, and Eq. (11) is then transformed into

$$\dot{R} = -AR + BR^{1/2} + C. \qquad (19)$$

Taking the values of related dynamic variables of the crack tip for $Mg_{65}Cu_{25}Gd_{10}$ into Eq. (19) and introducing two new variables: the reduced crack tip curvature radius $R'_{tip} = 10^8 R_{tip}$ and the reduced time $t' = 10^9 t$, Eq. (19) is then transformed into

$$\frac{dR'}{dt'} = -123.67R' + 250.45R'^{1/2} + 8.4. \qquad (20)$$

Fig. 6 illustrates the qualitative evolution of the R'_{tip} with the increase of the reduced time t' when the R^0_{tip} gets the values of 50 nm and 10 nm, corresponding to the above and below R^*_{tip} ($=39$ nm). When $R^0_{tip} > R^*_{tip}$, the crack tip sharpens, and the R_{tip} decreases; when $R^0_{tip} < R^*_{tip}$, the crack tip blunts, and the R_{tip} increases. Based on the experimental results of the evolution of the crack tip and the pattern transition among different fracture patterns in Fig. 2, we infer that the crack tip sharpening originated from the nano-scale plasticity at crack tip in this model which leads to the fracture pattern transition from the dimple structures to the periodic corrugations during fracture in MGs.
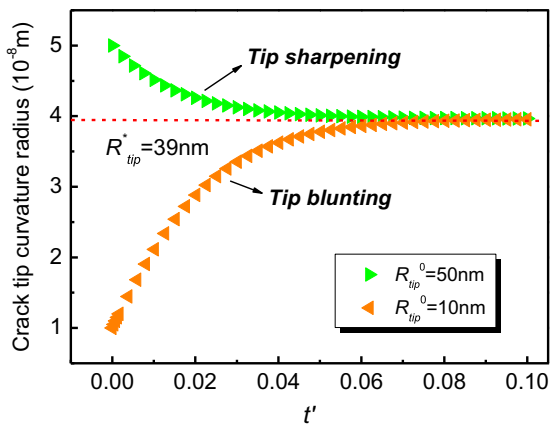
Fig. 6. Crack tip curvature radius evolution during fracture with the initial crack tip curvature radius $R^0_{tip} = 50$ nm and 10 nm. The red dashed line represents the stable crack tip curvature radius. (For interpretation of the references to color in this figure legend, the reader is referred to the web version of this article.)
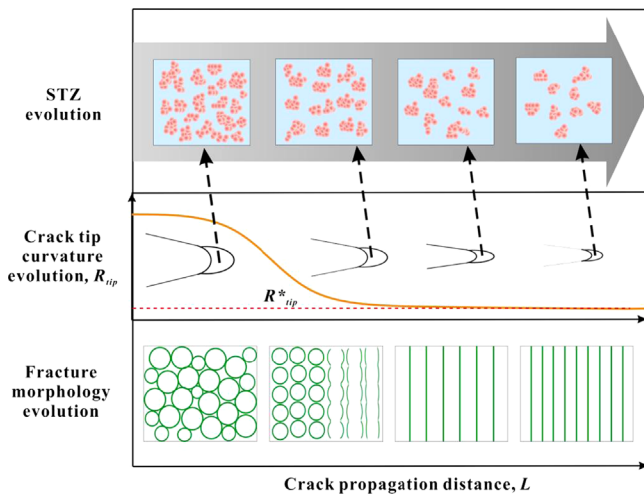
Fig. 7. Scheme of STZs evolution in plastic zone at crack tip, crack tip curvature evolution and fracture morphology evolution with the crack propagation distance, L.

For the predicted crack tip blunting behavior deduced from our model, it may explain the prior formation of the periodical stripes rather than the dimple structures in the initial stage of fracture for samples without pre-notches in the three bending test [25]. For samples without notches, small cavitations with nano-scale size form firstly as the seed cracks and the radius of the seed cracks are generally smaller than the critical crack tip curvature radius. Then the tip radius of these cavitations becomes bigger during plastic deformation at crack tip, which causes the crack tip to blunt, and these cavitations self-organize into periodical stripes. When the crack tip curvature radius is close to the R^*_{tip}, the periodic stripe pattern is replaced by the dimple pattern.

To show clearly the relationship between the STZ and the fracture morphology, the scheme of STZs evolution in plastic zone at crack tip, crack tip curvature evolution and fracture morphology evolution with the crack propagation distance, L, is shown in Fig. 7. From Fig. 7, one can see that STZs in the plastic zone at crack tip evolves during the whole crack propagation and the spatial distribution of STZs becomes sparse, leading to the dynamic evolution of the crack tip curvature radius. Based on the above analysis, the dynamic evolution of the crack tip curvature radius induces the fracture morphology transition on the fracture surface when R_{tip} is close to the critical value R^*_{tip}.

3.3.5. Contrasting the crack tip curvature radius with the activation energy of STZs in metallic glasses with different fracture toughness

To understand the different fracture behaviors of metallic glasses with different fracture toughness, we also contrast the R^*_{tip} and the activation energy of STZs, E_{STZ}, with MGs of different fracture toughness in Fig. 8. As is shown by the red dashed arrow line in Fig. 8, the R^*_{tip} displays a downward trend with the increase of the E_{STZ}. This result indicates that the tough MGs such as Zr-based MGs with higher values of E_{STZ} compared to those of brittle MGs and micro-scale local plastic zone [18] have lower R^*_{tip} value, and their crack propagation process finishes before the R_{tip} reaches the critical value R^*_{tip}. This is the reason why the dimple patterns are the main fracture morphology in tough MGs [28] rather than the appearance of the pattern transition. This explains why the fracture pattern transition from the dimple structures to the periodic corrugations is prone to occur in fracture surface of brittle MGs. Based on the above analysis, one might modulate the activation energy or density of STZs in MGs to get the tunable micro-scale and nano-scale fracture structures by micro-alloying and structural relaxation [37,38], which needs further research in future. The results also imply that the fracture behaviors of MGs
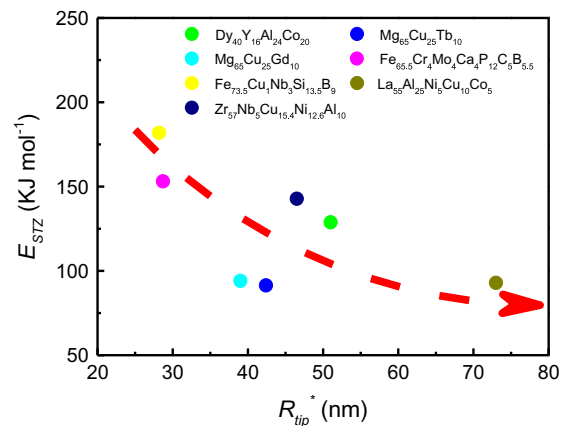
Fig. 8. The relationships of critical crack tip curvature radius R^*_{tip} and activation energy of STZs E_{STZ}. The red dashed arrow line represents the downward trend with the increase of E_{STZ}. (For interpretation of the references to color in this figure legend, the reader is referred to the web version of this article.)

are closely related to their intrinsic heterogeneous structure and flow units in metallic glasses [39–45], which provides useful insight into the structural origin of the fracture process and crack evolution in MGs.

4. Conclusions

(1) Various fracture morphologies in fracture surface of $Mg_{65}Cu_{25}$-Gd_{10} were studied systematically and quantitatively by SEM and AFM. A new experimental parameter – the critical crack tip curvature radius – was proposed, which can clearly reveal the dynamic evolution of crack propagation and control the pattern transition among different fracture morphologies of brittle MGs.

(2) To simulate the crack propagation process and predict the critical crack tip curvature radius, the proposed microscopic theoretical model of the crack tip curvature radius evolution based on the STZ theory was developed. The crack tip sharpening and the crack tip blunting phenomena from the model explain appropriately the pattern transition from the dimple structures to the periodic corrugations and from the nano-scale cavitations to the periodic corrugations.

(3) By contrasting the critical crack tip curvature radii with the activation energy of STZs of metallic glasses with different fracture toughness, the fracture pattern transition among various fracture patterns is prone to take place in brittle MGs with the higher activation energy of STZs. It indicates that the controllable fracture structure may be obtained by tuning the activation energy and the density of STZs, which relates the fracture behavior to the heterogeneous structure of MGs.

Acknowledgments

References

[1] M.C. Cross, P.C. Hohenberg, Rev. Mod. Phys. 65 (1993) 851–1112.
[2] B.T. Werner, Science 284 (1999) 102–104.
[3] M. Cross, H. Greenside, Pattern Formation and Dynamics in Nonequilibrium Systems, 1st ed., Cambridge University Press, New York, 2009.
[4] J. Fineberg, M. Marder, Phys. Rep. 313 (1999) 1–108.
[5] J.P. Guin, S.M. Wiederhorn, Phys. Rev. Lett. 92 (2004) 215502.
[6] E. Sharon, G. Cohen, J. Fineberg, Nature 410 (2001) 68–71.
[7] L.S. Aranson, L.S. Tsimring, Rev. Mod. Phys. 78 (2006) 641–692.
[8] X.K. Xi, D.Q. Zhao, M.X. Pan, W.H. Wang, Y. Wu, J.J. Lewandowski, Phys. Rev. Lett. 94 (2005) 125510.
[9] G. Wang, Y.T. Wang, Y.H. Liu, M.X. Pan, D.Q. Zhao, W.H. Wang, Appl. Phys. Lett. 89 (2006) 121909.
[10] A.S. Argon, Acta Metall. 27 (1979) 47–58.
[11] G. Wang, D.Q. Zhao, H.Y. Bai, M.X. Pan, A.L. Xia, B.S. Han, X.K. Xi, Y. Wu, W.H. Wang, Phys. Rev. Lett. 98 (2007) 235501.
[12] M.L. Falk, J.S. Langer, Phys. Rev. E 57 (1998) 7192–7205.
[13] J.S. Langer, Phys. Rev. E 70 (2004) 041502.
[14] M.L. Falk, J.S. Langer, Annu. Rev. Condens. Matter Phys. 2 (2011) 353–373.
[15] E. Bouchbinder, A. Pomyalov, I. Procaccia, Phys. Rev. Lett. 97 (2006) 134301.
[16] C.H. Rycroft, E. Bouchbinder, Phys. Rev. Lett. 109 (2012) 194301.
[17] M. Gao, B.A. Sun, C.C. Yuan, J. Ma, W.H. Wang, Acta Mater. 60 (2012) 6952–6960.
[18] H.B. Yu, W.H. Wang, H.Y. Bai, Phys. Rev. B 81 (2010) 220201.
[19] H.B. Yu, X. Shen, Z. Wang, L. Gu, W.H. Wang, H.Y. Bai, Phys. Rev. Lett. 108 (2012) 015504.
[20] Y.T. Wang, G. Wang, X.X. Xia, W.H. Wang, J. Appl. Phys. 106 (2009) 113528.
[21] M.Q. Jiang, Z. Ling, J.X. Meng, J.B. Gao, L.H. Dai, Scr. Mater. 62 (2010) 572–575.
[22] X.X. Xia, W.H. Wang, Small 8 (2012) 1197–1203.
[23] A. Livne, E. Bouchbinder, I. Svetlizky, J. Fineberg, Science 327 (2010) 1359–1363.
[24] M. Adda-Bedia, R.E. Arias, E. Bouchbinder, E. Katzav, Phys. Rev. Lett. 110 (2013) 014302.
[25] G. Wang, K.C. Chan, X.H. Xu, W.H. Wang, Acta Mater. 56 (2008) 5845–5860.
[26] E. Bouchaud, D. Boivin, J.L. Pouchou, D. Bonamy, B. Poon, G. Ravichandran, Europhys. Lett. 83 (2008) 66006.
[27] P.F. Guan, S. Lu, M.J.B. Spector, P.K. Valavala, M.L. Falk, Phys. Rev. Lett. 110 (2013) 185502.
[28] J.X. Meng, Z. Ling, M.Q. Jiang, H.S. Zhang, L.H. Dai, Appl. Phys. Lett. 92 (2008) 171909.
[29] P. Tandaiya, R. Narasimhan, U. Ramamurty, Acta Mater. 61 (2013) 1558–1570.
[30] A.E. Lobkovsky, J.S. Larger, Phys. Rev. E 58 (1998) 1568–1576.
[31] J.S. Larger, A.E. Lobkovsky, Phys. Rev. E 60 (1999) 6978–6983.
[32] J.S. Larger, Phys. Rev. E 62 (2000) 1351–1360.
[33] N.I. Muskhelishvili, Some Basic Problems of the Mathematical Theory of Elasticity, 2nd ed., Noordhoff International Publishing, Netherland, 1977.
[34] W.L. Johnson, K. Samwer, Phys. Rev. Lett. 95 (2005) 195501.
[35] W.H. Wang, Prog. Mater. Sci. 57 (2012) 487–656.
[36] X.K. Xi, D.Q. Zhao, M.X. Pan, W.H. Wang, Y. Wu, J.J. Lewandowski, Appl. Phys. Lett. 89 (2006) 181911.
[37] G.R. Garrett, M.D. Demetriou, J. Chen, W.L. Johnson, Appl. Phys. Lett. 101 (2012) 241913.
[38] W. Jiao, P. Wen, H.L. Peng, H.Y. Bai, B.A. Sun, W.H. Wang, Appl. Phys. Lett. 102 (2013) 101903.
[39] M.D. Demetriou, D.C. Hofmann, W.L. Johnson, R.O. Ritchie, Nat. Mater. 10 (2011) 123–128.
[40] W.H. Wang, J. Appl. Phys. 110 (2011) 053521.
[41] R.O. Ritchie, Nat. Mater. 10 (2011) 817–822.
[42] S.T. Liu, W. Jiao, B.A. Sun, W.H. Wang, J. Non-Cryst. Solids 376 (2013) 76–80.
[43] Z. Wang, P. Wen, L.S. Huo, H.Y. Bai, W.H. Wang, Appl. Phys. Lett. 101 (2012) 121906.
[44] D.P. Wang, D.Q. Zhao, D.W. Ding, H.Y. Bai, W.H. Wang, J. Appl. Phys. 115 (2014) 123507.
[45] H.L. Peng, M.Z. Li, W.H. Wang., Phys Rev Lett. 106 (2011) 135503.